

Iterative Design of a 60 kW All-Si Modular LLC Converter for Electric Vehicle Ultra-Fast Charging

Original

Iterative Design of a 60 kW All-Si Modular LLC Converter for Electric Vehicle Ultra-Fast Charging / Cittanti, D., Vico, E., Gregorio, M., Mandrile, F., Bojoi, R.. - (2020), pp. 1-6. (2020 AEIT International Conference of Electrical and Electronic Technologies for Automotive (AEIT AUTOMOTIVE)) [10.23919/AEITAUTOMOTIVE50086.2020.9307381].

Availability:

This version is available at: 11583/2866092 since: 2021-01-23T11:20:45Z

Publisher:

IEEE

Published

DOI:10.23919/AEITAUTOMOTIVE50086.2020.9307381

Terms of use:

This article is made available under terms and conditions as specified in the corresponding bibliographic description in the repository

Publisher copyright

IEEE postprint/Author's Accepted Manuscript

©2020 IEEE. Personal use of this material is permitted. Permission from IEEE must be obtained for all other uses, in any current or future media, including reprinting/republishing this material for advertising or promotional purposes, creating new collecting works, for resale or lists, or reuse of any copyrighted component of this work in other works.

(Article begins on next page)

Iterative Design of a 60 kW All-Si Modular LLC Converter for Electric Vehicle Ultra-Fast Charging

Davide Cittanti, Enrico Vico, Matteo Gregorio, Fabio Mandrile and Radu Bojoi

Department of Energy “G. Ferraris”

Politecnico di Torino

Torino, Italy

davide.cittanti@polito.it

Abstract—This paper proposes an iterative design procedure for a high-power LLC resonant converter, taking part in a 60 kW modular DC/DC conversion stage for an electric vehicle (EV) ultra-fast battery charger. The basics of operation of the LLC converter are briefly recalled and the most relevant analytical expressions are reported. Due to the high-power requirement and the wide output battery voltage range (i.e. 250-1000 V), a modular design approach is adopted, leveraging the split input DC-link structure provided by a 3-level active front-end. A total of four modules, with at 15 kW nominal power and a 250-500 V output voltage regulation capability, are designed with a straightforward iterative procedure based on the first-harmonic approximation (FHA). Finally, the proposed methodology is verified experimentally on a 15 kW LLC converter prototype directly resulting from the design procedure.

Index Terms—LLC resonant converter, isolated DC/DC converters, battery chargers, electric vehicles (EV)

I. INTRODUCTION

The main requirements for an electric vehicle (EV) ultra-fast battery charger can be identified in high power density, high efficiency, low grid current distortion, wide input/output voltage range and low battery current ripple. DC fast chargers are generally composed of two different conversion stages interconnected by a DC-link [1], as shown in Fig. 1: an AC/DC converter with power factor correction (PFC) capability and an isolated DC/DC converter which provides galvanic isolation between the low-voltage grid and the battery. This work focuses only on the DC/DC conversion stage.

It is well known that resonant converters represent excellent candidates for high-frequency DC/DC conversions, as soft-switching operation enables high efficiency and limited EMI noise emission [2]. Moreover, operating at high switching frequencies allows to reduce both size and weight of resonant and/or filtering components, such as capacitors, inductors and transformers, theoretically leading to higher power-density converters. Nevertheless, special care must be observed when designing and realizing magnetic components for such high frequencies, since shrinking size and loss increase can easily lead to exceed the thermal limits.

Since conventional unidirectional resonant converters (i.e. series-resonant and parallel-resonant) lack wide load/voltage regulation capabilities [2], they are not suitable for battery charging applications. This limitation is overcome by the LLC resonant converter, which allows to regulate the load in a wide output voltage range with a relatively narrow switching frequency variation [3], [4].

Design methodologies for LLC converters have been widely explored in literature, mainly regarding power applications up to the kW range [5]–[15]. In particular, [11]–[16] focus on LLC designs for EV battery chargers.

For instance, iterative design procedures are proposed in [7] and [8], however targeting power ratings lower than

250 W. [12] reports a design method which guarantees the LLC zero-voltage switching (ZVS) operation considering the worst-case operating point defined by the non-linear charging characteristic of a battery. Moreover, [13] suggests a detailed design procedure which focuses on the optimization of the high-frequency transformer parameters.

Even though [16] reports a 10 kW LLC converter prototype, as of the authors’ best knowledge, high-power LLC converter designs are extremely rare in literature. Accordingly, the goal of this paper is to propose a straightforward iterative design procedure for a high-power LLC converter for battery charging applications, aimed at minimizing the total converter conduction losses. Silicon (Si) technology is adopted for all semiconductor devices (i.e. input bridge MOSFETs and output rectification diodes), due to its reliability, high maturity and low-cost, which are all desirable features for battery chargers. Moreover, the proposed LLC converter design is characterized by a modular structure, to enable both easy scalability and the series/parallel reconfiguration of the converter modules, which narrows the output voltage regulation requirement of a single converter.

This paper is organized as follows. Section II describes the operational basics of the LLC resonant converter, reporting the most significant analytical expressions obtained with the first-harmonic approximation (FHA) method. In Section III the requirements and specifications of the proposed modular battery charger are detailed and an unconventional LLC converter structure is selected. An iterative design procedure for a single LLC module is developed and described, leading to an optimized converter design minimizing the total conduction losses. In Section IV the proposed design methodology is experimentally verified on a 15 kW LLC prototype. Finally, Section V summarizes and concludes this paper.

II. LLC BASICS OF OPERATION

This work considers a full-bridge LLC converter, schematically represented in Fig. 2. Differently from conventional pulse-width modulated (PWM) converters, the input bridge of the LLC is controlled with a fixed duty cycle to generate an alternating square-wave voltage. From a simplified sinusoidal perspective, the resonant tank, composed of a resonant capacitance C_r , a resonant inductance L_r and the magnetizing inductance of the transformer L_m , can be considered as a frequency-dependent equivalent impedance. By varying the switching frequency of the input bridge, the magnitude

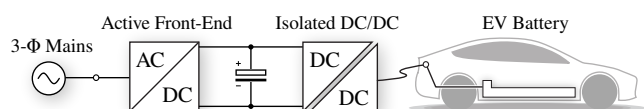


Fig. 1. Schematic overview of an EV ultra-fast DC charger.

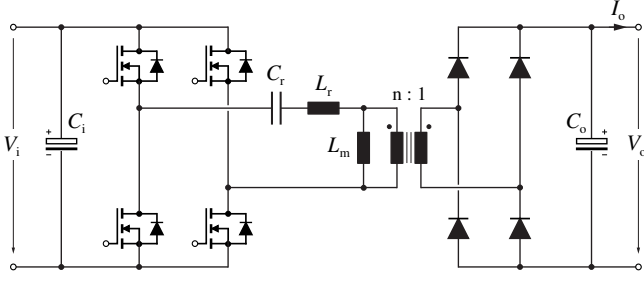


Fig. 2. Schematic of the considered full-bridge LLC resonant converter.

and phase of this impedance change, providing the ability to regulate the output voltage. Moreover, due to the high selectivity of the resonant tank impedance magnitude, the power transfer is dominated by the first-harmonic of the square-wave input voltage, thus simplifying the analysis of the converter (i.e. FHA [3]).

A set of parameters needs to be defined to simplify the following analysis and design procedure:

- Inductance ratio $\lambda = \frac{L_r}{L_m}$
- Primary resonance frequency $f_{r,I} = \frac{1}{2\pi\sqrt{L_r C_r}}$
- Secondary resonance frequency $f_{r,II} = \frac{1}{2\pi\sqrt{(L_r + L_m)C_r}}$
- Normalized switching frequency $f_n = \frac{f_{sw}}{f_{r,I}}$
- Characteristic impedance $Z_r = \sqrt{\frac{L_r}{C_r}}$
- Output/input voltage gain $M = \frac{nV_o}{V_i}$
- Quality factor $Q = \frac{\pi^2 Z_r I_o}{8 n^2 V_o} = \frac{\pi^2 Z_r}{8 n^2 R_o}$

where n is the transformer turns ratio, f_{sw} is the switching frequency of the input bridge and $R_o = V_o/I_o$ is the equivalent output load resistance.

By analysing with FHA the impedance divider between the resonant tank and R_o , the converter gain expression is found [5]:

$$M(f_n, \lambda, Q) = \frac{1}{\sqrt{\left(1 + \lambda - \frac{\lambda}{f_n^2}\right)^2 + Q^2 \left(f_n - \frac{1}{f_n}\right)^2}}. \quad (1)$$

As expected, once the converter design is defined (i.e. λ , f_r and Z_r are fixed), the voltage gain depends on the switching frequency, which represents the control parameter. However, the further dependency of M on the output load (i.e. related to Q) complicates both the design and the control of the LLC converter. The voltage gain dependence on f_n and Q for $\lambda = 0.1$ is graphically illustrated in Fig. 3(a).

Since the LLC converter should always operate the input bridge MOSFETs in ZVS conditions to minimize switching losses, the analysis of the equivalent impedance seen from the input bridge perspective is of interest. The expression of this impedance can also be derived by leveraging FHA:

$$Z(f_n, \lambda, Q) = Z_r \left[\frac{f_n^2 Q}{\lambda^2 + f_n^2 Q^2} + j \left(\frac{\lambda f_n}{\lambda^2 + f_n^2 Q^2} - \frac{1 - f_n^2}{f_n} \right) \right]. \quad (2)$$

The input impedance magnitude and phase dependence on f_n and Q for $\lambda = 0.1$ is graphically shown in Fig. 3(b).

The operating frequency range can be subdivided in three main regions. When the switching frequency is lower than $f_{r,II}$, the resonant tank impedance is always capacitive (i.e. negative phase). Vice-versa, the impedance is always inductive (i.e. positive phase) when $f_{sw} > f_{r,I}$. The third region is found in between, where the resonant tank impedance can be either capacitive or inductive, depending on the output load value. The two extremes are represented by the no-load or open-circuit condition ($Q=0$) and the infinite-load or short-circuit condition ($Q=\infty$). Identifying the input impedance nature is of utmost importance to ensure the ZVS operation of the input bridge. For instance, when the impedance is inductive, the current lags the input voltage square-wave, thus allowing the soft turn-off of the MOSFETs. The opposite is true in the capacitive region, which is characterized by hard-switching operation and must thus be avoided. Moreover, it is worth noting that the capacitive region is unstable from a control perspective [17], as the frequency-to-gain small-signal ratio is positive (i.e. opposite with respect to the inductive region), as shown by the curve slopes below M_{lim} in Fig. 3(a).

The load-independent expression of the boundary between capacitive and inductive regions is derived in [12], as

$$M_{lim}(f_n, \lambda) = \frac{f_n}{\sqrt{(1 + \lambda)f_n^2 - \lambda}}, \quad (3)$$

which is graphically represented in Fig. 3(a). Accordingly, the LLC design procedure must ensure that all converter operating points in the load-dependent region lay above M_{lim} .

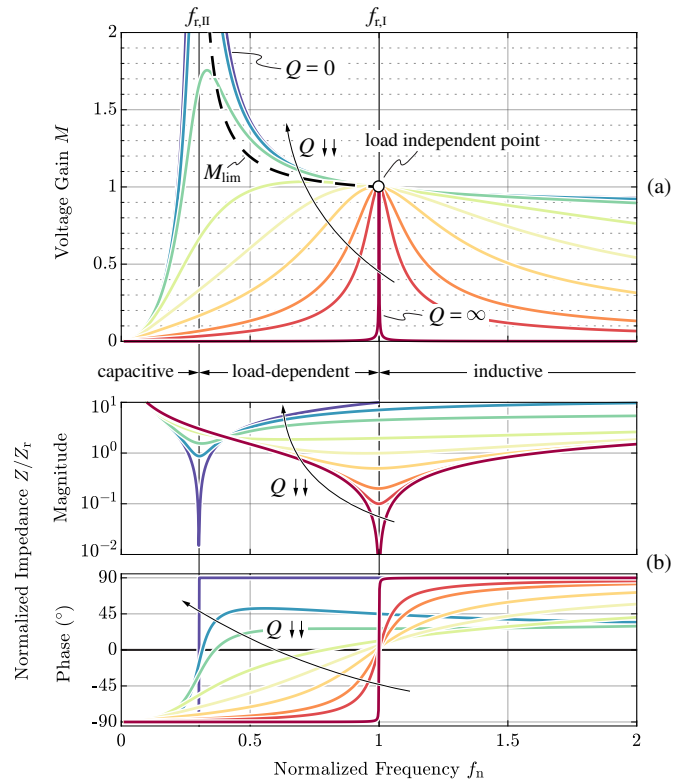


Fig. 3. LLC resonant converter gain M (a) and normalized input impedance Z/Z_r (b) for $\lambda = 0.1$, as a function of the normalized switching frequency f_n and the quality factor Q . The capacitive, inductive and load-dependent regions are indicated. The boundary gain curve M_{lim} between inductive and capacitive regions (i.e. ZVS limit) is highlighted.

III. DESIGN PROCEDURE

The present work considers a 60 kW DC fast charger, capable of operating within a 250 V – 1000 V output battery voltage range. Due to the high power requirement, the proposed DC/DC converter features a modular structure, leveraging the split DC-link provided by a 3-level AFE [18], as illustrated in Fig. 4(a). A total of four 15 kW LLC converter modules are designed and independently realized, splitting the power rating and allowing to turn-off one or more modules at light load operation, ensuring higher efficiency over the complete charging range. Moreover, the output of a module pair can be reconfigured to be either in parallel or in series with the other pair, depending on the required battery voltage. Overall, the operating region of the proposed modular battery charger is illustrated in Fig. 4(b), where the maximum converter output current I_{\max} , voltage V_{\max} and power P_{\max} limits are indicated.

Since each LLC converter is rated at 15 kW, to further reduce the ratings and physical size of the resonant tank components, the unconventional structure reported in Fig. 5 is adopted herein. Two transformers, series-connected at the primary side, feed two separate diode bridges at the secondary side, which are then connected in parallel. This allows to both downsize the single transformers and halve the current rating of the output rectification diodes, enabling the utilization of magnetic cores and semiconductor devices practically available on the market. To ensure the balanced operation of the converter, the resonant capacitor is connected between the transformers, while the resonant inductor is realized by coupling two separate windings on a single core, equally distributing the voltage drop between the two circuit paths leading to the transformers.

In general, the goal of an LLC design procedure is to identify the four parameters n , L_r , C_r and L_m which ensure the required converter input/output characteristics, while minimizing losses and/or the size of the passive components. Since the design methodology proposed in this work has

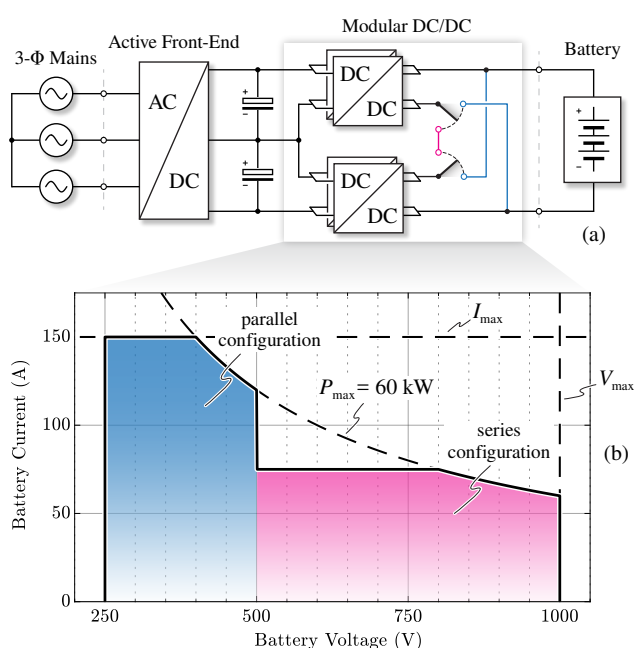


Fig. 4. Schematic overview of the proposed 60 kW modular DC fast charger (a). Highlight of the output voltage/current feasible operating region of the series/parallel reconfigurable DC/DC converter (b).

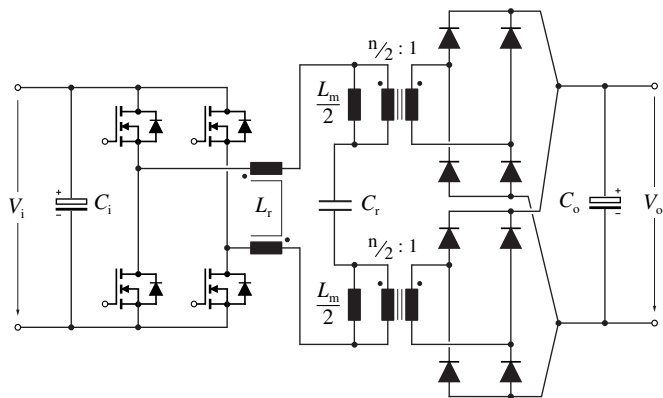


Fig. 5. Schematic overview of the adopted 15 kW LLC converter structure.

general validity, it is applied to the traditional LLC circuit shown in Fig. 2. Nevertheless, the parameters belonging to the unconventional LLC structure here adopted are simply derived from the relations reported in Fig. 5.

The proposed LLC iterative design procedure is composed of several steps, described in the following.

① Definition of the design specifications and constraints. The specifications of the LLC module considered in this work are reported in Table I. It is assumed that the converter input voltage V_i is adjusted by the AFE control between 325 V – 400 V, to minimize the required voltage gain range of the DC/DC stage [18]. Moreover, the converter operating frequency range is defined as 100 kHz – 250 kHz.

② Transformer turns ratio n selection. It is well known that resonance operation is normally the highest efficiency working point of the LLC converter, since no recirculation time is present, i.e. reducing conduction losses with respect to boost mode operation, and the rectifier diode reverse recovery is ideally eliminated, i.e. reducing switching losses with respect to buck mode operation. Therefore, resonance mode ($M = 1$) is targeted for the nominal operating conditions, i.e. $V_o = 400$ V. From the specifications reported in Table I, this is obtained for every value $n \leq V_{i,\max}/V_{o,\text{nom}} = 1$. Nevertheless, $n = 1$ is selected herein, since the transformer design is simplified, lending itself to straightforward primary/secondary winding interleaving, and the converter efficiency is maximized inside the 325 V – 400 V output window (650 V – 800 V when in series configuration), which covers the battery voltage range of most commercially available EVs [19], [20]. An overview of the input/output voltage gains obtained with $n = 1$ is reported in Fig. 6. The minimum gain $M_{\min} = 0.77$ and the maximum gain $M_{\max} = 1.25$ result.

③ Resonance frequency $f_{r,1}$ selection. This value is initialized as the maximum possible switching frequency, i.e. $f_{\text{sw,max}}$, however it is subject to iteration, as shown in the design flowchart of Fig. 7. In particular, $f_{r,1}$ is progressively

TABLE I. SPECIFICATIONS OF THE CONSIDERED 15 kW LLC MODULE.

Parameter	Description	Value
V_i	input voltage range	325...400 V
V_o	output voltage range	250...500 V
$V_{o,\text{nom}}$	nominal output voltage	400 V
$I_{o,\text{nom}}$	nominal output current	37.5 A
$P_{o,\text{nom}}$	nominal output power	15 kW
f_{sw}	switching frequency range	100...250 kHz

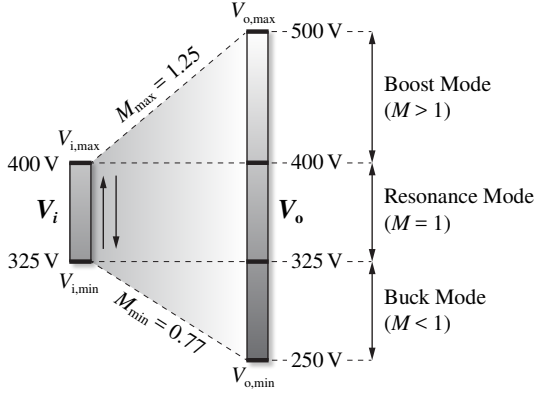


Fig. 6. LLC input/output voltage gain overview, considering $n = 1$. The input voltage V_i is adjusted by the AFE according to the output voltage V_o , in order to maximize the resonance mode operating region.

reduced with 10 Hz steps until the converter operating frequency range coincides with the one reported in Table I.

④ Minimum load Q_{\min} at minimum gain M_{\min} definition. To reduce the buck-mode frequency operating range of the converter, a minimum load at maximum frequency is considered. In this case, 25% of the nominal current is assumed as $I_{o,\min}$, since the modular charger is already split in four modules which can be selectively turned off at light load. Unfortunately, the minimum quality factor expression depends on the characteristic impedance of the resonant tank,

$$Q_{\min}(V_{o,\min}) = \frac{\pi^2 Z_r I_{o,\min}}{8 n^2 V_{o,\min}}, \quad (4)$$

therefore it is calculated by iterative means together with the two subsequent design steps.

⑤ Inductance ratio λ calculation. This value is found by forcing the Q_{\min} curve to pass through the point $(f_{sw,\max}, M_{\min})$ in the (f_{sw}, M) plane, inverting (1):

$$\lambda = \frac{f_{r,I}^2}{f_{r,I}^2 - f_{sw,\max}^2} \left[1 - \sqrt{\frac{1}{M_{\min}^2} - Q_{\min}^2 \left(\frac{f_{sw,\max}^2 - f_{r,I}^2}{f_{r,I} f_{sw,\max}} \right)^2} \right] \quad (5)$$

Higher values of λ provide an operational margin, however they lead to a lower L_m and thus higher circulating current.

⑥ Characteristic impedance Z_r calculation. Since the converter boost operation coincides with the power-limited region, the worst-case condition for achieving complete ZVS is found according to [12], by setting the tangency between the converter maximum power envelope and the inductive/capacitive region boundary curve M_{lim} . The impedance expression is derived, taking into account a predefined p.u. margin x for achieving ZVS, as

$$Z_r = (1 - x) \frac{8}{\pi^2} \frac{V_{i,\max}^2}{P_{o,nom}} \left[\lambda + \sqrt{\lambda(1 + \lambda)} \right]. \quad (6)$$

Lower values of Z_r provide an increased margin, however they lead to reduced L_r and L_m , increasing the circulating current, and to an increased C_r . The calculated Z_r is reiterated into ⑤, until a stable solution is obtained.

⑦ Maximum magnetizing inductance L_m verification. The ZVS of the primary bridge must be ensured also in buck mode operation at zero load, i.e. when only the transformer magnetizing current I_m is switched, since even a single hard-switching transition can be destructive for the MOSFETs. The worst-case is found when $f_{sw} = f_{sw,\max}$ and $Q = 0$, hence

the voltage gain M can be derived from (1). Nevertheless, to ensure a reasonable margin, $M = M_{\min}$ is assumed for the design. Therefore, being $C_{Q,eq}$ the charge-equivalent output capacitance of a single MOSFET [21], the magnetizing inductance must fulfill

$$L_m \leq \frac{t_{d,\max} M_{\min}}{8 C_{Q,eq}(V_{i,\min}) f_{sw,\max}} = L_{m,\max}, \quad (7)$$

where $t_{d,\max}$ is the maximum allowed dead-time. In the present case, to limit the recirculating time of the primary MOSFET body diodes, a dead-time equal to 10% of the minimum switching period, i.e. $t_{d,\max} = 400$ ns, is selected. Since Vishay SiHG018N60E MOSFETs (600 V, 21 m Ω) are selected due to their extremely low on-state resistance in a standard TO-247 package [22], $C_{Q,eq}(V_{i,\min}) = 1.8$ nF results and $L_m \leq 85.4$ μ H is obtained. If this limit is encountered, the iterative procedure is stopped and the resonant tank parameters are calculated according to

$$L_m = L_{m,\max}, \quad L_r = \lambda L_m, \quad C_r = \frac{1}{(2\pi f_{r,I})^2 L_r}. \quad (8)$$

⑧ Minimum operating frequency $f_{op,\min}$ calculation and verification. This value is calculated by numerical means, knowing λ , Z_r , $M = M_{\max}$ and $Q = Q(V_{o,\max}, P_{o,nom})$, and inverting equation (1). If $f_{op,\min} > f_{sw,\min}$, then the procedure is repeated, restarting from step ③ with a progressively lower $f_{r,I}$ value. Otherwise, the iterative design procedure is stopped and the last step is entered.

⑨ Resonant tank parameters L_r , C_r , L_m calculation:

$$L_r = \frac{Z_r}{2\pi f_{r,I}}, \quad C_r = \frac{1}{2\pi f_{r,I} Z_r}, \quad L_m = \frac{1}{\lambda} \frac{Z_r}{2\pi f_{r,I}}. \quad (9)$$

The proposed iterative design procedure aims to minimize the conduction losses of the semiconductor devices and the

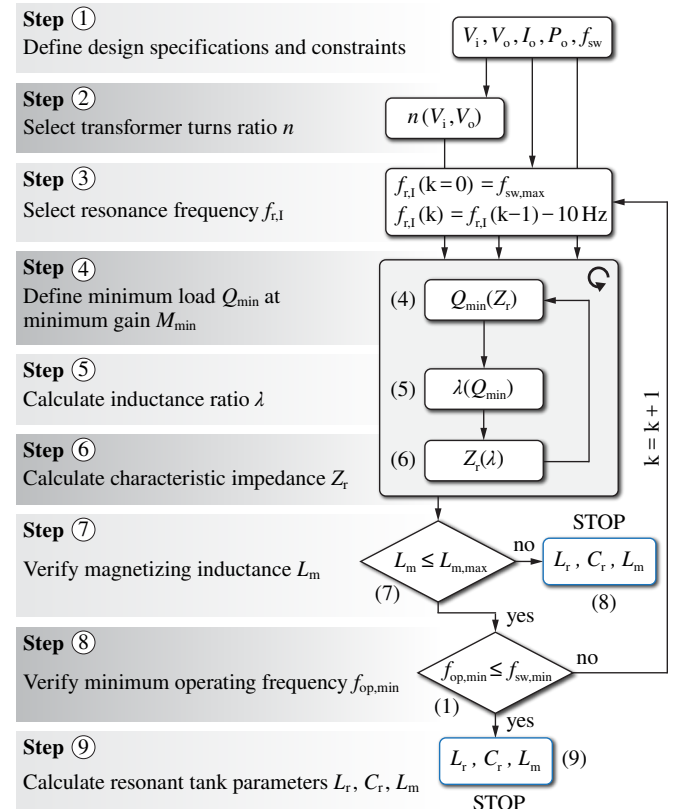


Fig. 7. Flowchart of the proposed iterative design procedure.

winding losses of the magnetic components. Therefore, the final design must minimize the transformer peak magnetizing current I_m , which doesn't contribute to the power transfer, and tighten the boost-mode operating region, to avoid large recirculation times. It is simply derived that, at resonance,

$$I_m = \frac{n V_o}{4 f_{r,I} L_m}. \quad (10)$$

By substituting (6) into (9), then (9) into (10),

$$I_m \propto \frac{\lambda}{\lambda + \sqrt{\lambda(1+\lambda)}} \quad (11)$$

is obtained, which is monotonically increasing with λ . Therefore, since the required λ decreases by lowering $f_{r,I}$ according to (5) (the further is $f_{r,I}$ from $f_{sw,max}$, the flatter the Q curves can be), it is clear that the lowest I_m is obtained when the converter operating region fits the complete switching frequency range selected in step ①. Moreover, decreasing $f_{r,I}$ also minimizes the frequency width of the boost-mode region, leading to an overall conduction loss optimal design. These considerations are verified in Fig. 8, which shows the simulated LLC resonant tank RMS current over the full operating region according to three different designs increasingly exploiting the available switching frequency range.

With the input specifications of Table I and considering a ZVS load margin of $x = 5\%$, the proposed design procedure results in $L_r = 9.0 \mu\text{H}$, $C_r = 141.8 \text{ nF}$ and $L_m = 28.2 \mu\text{H}$, being $f_{r,I} = 140.5 \text{ kHz}$, $\lambda = 0.32$ and $Z_r = 8.0 \Omega$. The selected margin assumes that the capacitor value may vary in a $\pm 5\%$ window, i.e. due to manufacturing tolerances, and the resonant/magnetizing inductance values can be tuned to keep the desired $f_{r,I}$, i.e. thus varying Z_r and the worst-case Q for ZVS by $\pm 5\%$. The operating region of the designed LLC converter is illustrated in Fig. 9.

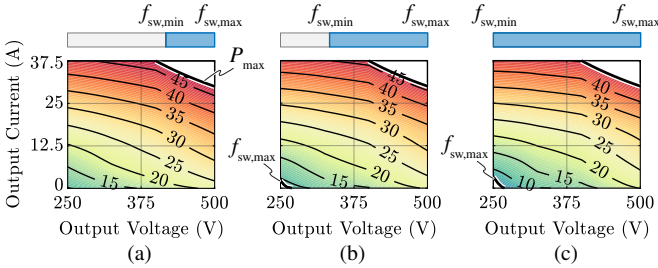


Fig. 8. Simulated resonant tank RMS current (A) over the complete operating range in three different design conditions: $f_{sw,min} = 200 \text{ kHz}$ (a), $f_{sw,min} = 150 \text{ kHz}$ (b) and $f_{sw,min} = 100 \text{ kHz}$ (c). The minimum current stresses are obtained when the full switching frequency range is exploited.

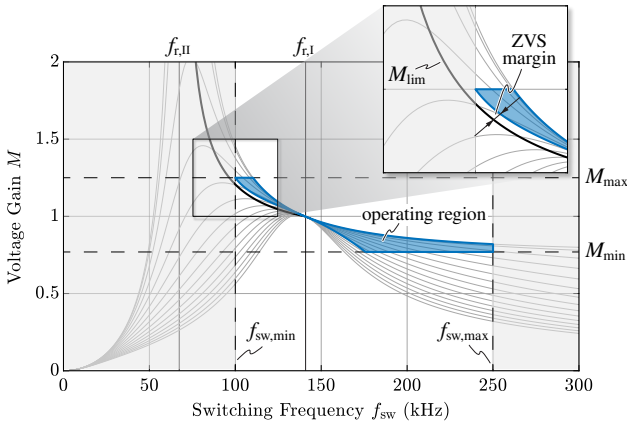


Fig. 9. Operating region of the designed LLC converter, with highlight of the selected ZVS margin in boost mode operation.

TABLE II. LLC CONVERTER PARAMETERS AND COMPONENT VALUES.

Parameter	Description	Value
n	transformer turns ratio	1
L_r	resonant inductance	$8.7 \mu\text{H}$
C_r	resonant capacitance	147.0 nF
L_m	magnetizing inductance	$25.3 \mu\text{H}$
C_i	input filter capacitance	$70 \mu\text{F}$
C_o	output filter capacitance	$220 \mu\text{F}$
$f_{r,I}$	primary resonance frequency	140.6 kHz
$f_{r,II}$	secondary resonance frequency	71.2 kHz
λ	inductance ratio	0.34
Z_r	characteristic impedance	7.7Ω

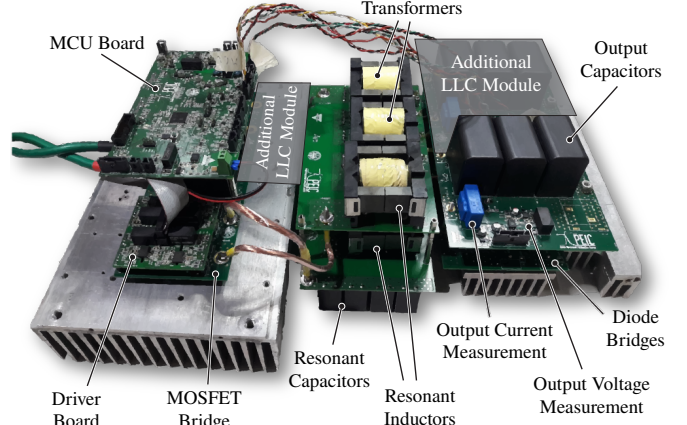


Fig. 10. Overview of the realized LLC converter prototype, in an early testing stage. Since the boards are designed for two paralleled 15 kW modules, the parts belonging to the second module are greyed out.

IV. EXPERIMENTAL VERIFICATION

A prototype of a single 15 kW converter module, illustrated in Fig. 10, is realized for testing purposes. The equivalent circuit parameters of the converter are reported in Table II. Since the resonant capacitance value is $\approx 4\%$ higher than the desired value, L_r is adjusted to maintain the specified resonance frequency. As a consequence, Z_r is reduced, i.e. leading to a larger ZVS margin. Moreover, L_m is adjusted to obtain the desired λ value, with a slight additional margin.

The converter primary and secondary resonance frequencies are measured experimentally with a HIOKI 3532-50 LCR meter [23], as illustrated in Fig. 11. $f_{r,I}$ and $f_{r,II}$ are obtained by short-circuiting and disconnecting the secondary side of the transformers, respectively. In this way, an equivalent infinite-load and zero-load conditions are simulated.

Since at the time of writing the converter prototype is in an early testing phase (e.g. general purpose passively cooled heatsinks are adopted), it is operated at reduced voltage and current values with respect to the ratings reported in Table I.

To verify the ZVS operation of the converter, a highlight of a switching transition of the primary MOSFET bridge operated in resonance-mode is provided in Fig. 12. It is

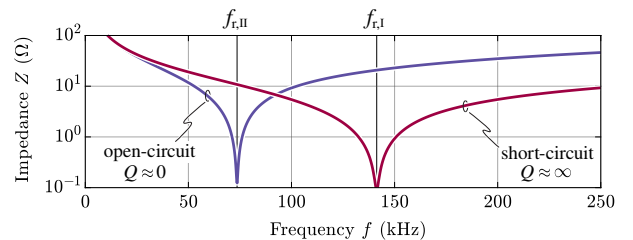


Fig. 11. Measured LLC resonant tank impedance with transformer secondary in open circuit ($Q \approx 0$) and in short-circuit ($Q \approx \infty$).

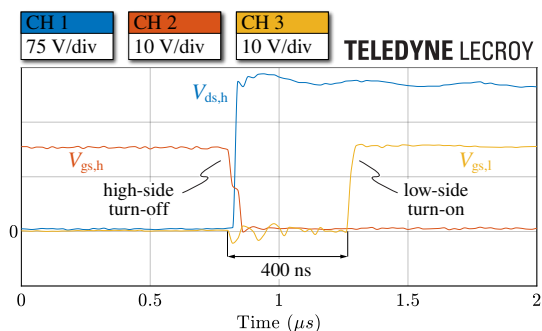


Fig. 12. High-side MOSFET drain-source voltage $V_{ds,h}$ and high-side/low-side MOSFET gate-source voltages $V_{gs,h}/V_{gs,l}$ during a ZVS transition at $V_i = 200$ V, $V_o = 200$ V and $I_o = 5$ A. A dead-time of 400 ns is adopted.

observed that the magnetizing current allows to complete the voltage transition ($V_i = 200$ V) before the switching dead-time is over, thus ensuring full ZVS.

Several tests are performed in different operating conditions and the measured resonant tank voltage V_r and current I_r are reported in Fig. 13. Resonance (a), boost (b) and buck (c) operating modes are preliminary verified, showing that in all cases complete ZVS operation is achieved (i.e. the switched current has the same sign as the switched voltage before the transition), hence supporting the design procedure.

V. CONCLUSION

This paper has proposed an iterative design procedure for an LLC resonant converter intended for EV battery charging applications. The operational basics of the converter have been introduced and the most important aspects for the converter design have been remarked. A 60 kW modular structure for EV ultra-fast charging has been proposed, leveraging four independent DC/DC modules which can be reconfigured in series/parallel according to the output battery voltage. Moreover, an unconventional LLC circuit topology has been adopted, to further reduce the power ratings of the single components. An iterative design procedure, aiming to minimize the converter conduction losses, has been proposed and applied to a 15 kW converter module with a 250–500 V output voltage range. Based on the derived specifications, an LLC converter prototype has been built and preliminary test results have supported the validity of the proposed design methodology.

REFERENCES

- [1] H. Tu, H. Feng, S. Srdic, and S. Lukic, "Extreme fast charging of electric vehicles: a technology overview," *IEEE Transactions on Transportation Electrification*, vol. 5, no. 4, pp. 861–878, Dec. 2019.
- [2] R. Steigerwald, "A comparison of half-bridge resonant converter topologies," *IEEE Transactions on Power Electronics*, vol. 3, no. 2, pp. 174–182, Apr. 1988.
- [3] T. Duerbaum, "First harmonic approximation including design constraints," in *Proc. of the International Telecommunications Energy Conference (INTELEC)*, San Francisco, CA, USA, 1999, pp. 321–328.
- [4] J. Lazar and R. Martinelli, "Steady-state analysis of the LLC series resonant converter," in *Proc. of the IEEE Applied Power Electronics Conference and Exposition (APEC)*, vol. 2, Anaheim, CA, USA, Mar. 2001, pp. 728–735.
- [5] S. De Simone, C. Adragna, C. Spini, and G. Gattavari, "Design-oriented steady-state analysis of LLC resonant converters based on FHA," in *Proc. of the International Symposium on Power Electronics, Electrical Drives, Automation and Motion (SPEEDAM)*, Taormina, Italy, May 2006, pp. 200–207.
- [6] B. Lu, W. Liu, Y. Liang, F. Lee, and J. van Wyk, "Optimal design methodology for LLC resonant converter," in *Proc. of the IEEE Applied Power Electronics Conference and Exposition (APEC)*, Dallas, TX, USA, Mar. 2006, pp. 533–538.
- [7] H. Choi, "Design considerations for an LLC resonant converter," in *Proc. of the Fairchild Power Seminar*, 2007, pp. 1–9.

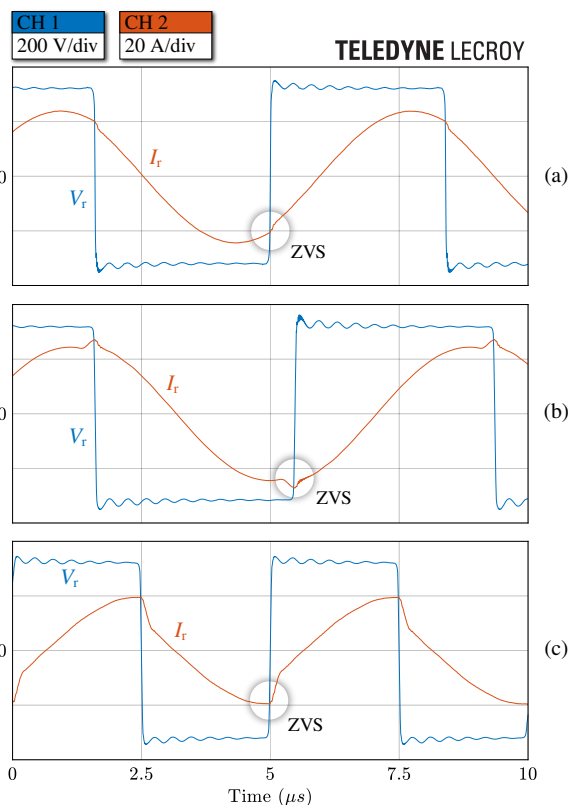


Fig. 13. Resonant tank voltage V_r and current I_r in (a) resonance mode ($f_{sw} = f_{r1}$), (b) boost mode ($f_{sw} = 130$ kHz) and (c) buck mode ($f_{sw} = 200$ kHz) with $V_i = 325$ V.

- [8] S. Abdel-Rahman, "Resonant LLC converter: operation and design," *Application Note*, pp. 1–19, 2012.
- [9] R. Yu, G. K. Y. Ho, B. M. H. Pong, B. W.-K. Ling, and J. Lam, "Computer-aided design and optimization of high-efficiency LLC series resonant converter," *IEEE Transactions on Power Electronics*, vol. 27, no. 7, pp. 3243–3256, Jul. 2012.
- [10] X. Fang, H. Hu, F. Chen, U. Somani, E. Auadisman, J. Shen, and I. Batarseh, "Efficiency-oriented optimal design of the LLC resonant converter based on peak gain placement," *IEEE Transactions on Power Electronics*, vol. 28, no. 5, pp. 2285–2296, May 2013.
- [11] F. Musavi, M. Craciun, D. S. Gautam, W. Eberle, and W. G. Dunford, "An LLC resonant DC-DC converter for wide output voltage range battery charging applications," *IEEE Transactions on Power Electronics*, vol. 28, no. 12, pp. 5437–5445, Dec. 2013.
- [12] J. Deng, S. Li, S. Hu, C. C. Mi, and R. Ma, "Design methodology of LLC resonant converters for electric vehicle battery chargers," *IEEE Transactions on Vehicular Technology*, vol. 63, no. 4, pp. 1581–1592, May 2014.
- [13] H. Wang, S. Dusmez, and A. Khaligh, "Design and analysis of a full-bridge LLC-based PEV charger optimized for wide battery voltage range," *IEEE Transactions on Vehicular Technology*, vol. 63, no. 4, pp. 1603–1613, May 2014.
- [14] Z. Fang, T. Cai, S. Duan, and C. Chen, "Optimal design methodology for LLC resonant converter in battery charging applications based on time-weighted average efficiency," *IEEE Transactions on Power Electronics*, vol. 30, no. 10, pp. 5469–5483, Oct. 2015.
- [15] C.-C. Hua, Y.-H. Fang, and C.-W. Lin, "LLC resonant converter for electric vehicle battery chargers," *IET Power Electronics*, vol. 9, no. 12, pp. 2369–2376, 2016.
- [16] H. Bai *et al.*, "Design of an 11 kW power factor correction and 10 kW ZVS DC/DC converter for a high-efficiency battery charger in electric vehicles," *IET Power Electronics*, vol. 5, no. 9, pp. 1714–1722, Nov. 2012.
- [17] D. Cittanti, M. Gregorio, E. Armando, and R. Bojoi, "Digital multi-loop control of an LLC resonant converter for electric vehicle DC fast charging," in *Proc. of the IEEE Energy Conversion Congress and Exposition (ECCE)*, Oct. 2020, pp. 4423–4430.
- [18] D. Cittanti, M. Gregorio, and R. Bojoi, "Digital Multi-Loop Control of a 3-Level Rectifier for Electric Vehicle Ultra-Fast Battery Chargers," in *Proc. of AEIT International Annual Conference (AEIT)*, Sep. 2020.
- [19] *Tesla Model 3 Owner's Manual*, Tesla, 2020.
- [20] *Porsche Taycan Models*, www.porsche.com, accessed: 2020-07-27.
- [21] M. Kasper, R. M. Burkart, G. Deboy, and J. W. Kolar, "ZVS of power MOSFETs revisited," *IEEE Transactions on Power Electronics*, vol. 31, no. 12, pp. 8063–8067, Dec. 2016.
- [22] *SiHG018N60E*, Vishay Semiconductors, Feb. 2019.
- [23] *3532-50 LCR Hi-Tester*, HIOKI, Jun. 2001.